Elastic wave-equation reflection traveltime inversion using dynamic warping and wave mode decomposition

Tengfei Wang, Jiubing Cheng, Qiang Guo and Chenlong Wang

May 21, 2017

Summary

Elastic full waveform inversion (EFWI) provides high-resolution parameter estimation of the subsurface but requires good initial guess of the true model. The traveltime inversion only minimizes traveltime misfits which are more sensitive and linearly related to the low-wavenumber model perturbation. Therefore, building initial P and S wave velocity models for EFWI by using elastic wave-equation reflections traveltime inversion (WERTI) would be effective and robust, especially for the deeper part. In order to distinguish the reflection travletimes of P or S-waves in elastic media, we decompose the surface multi-component data into vector P- and S-wave seismogram. We utilize the dynamic image warping to extract the reflected P- or S-wave traveltimes. The P-wave velocity are first inverted using P-wave traveltime followed by the S-wave velocity inversion with S-wave traveltime, during which the wave mode decomposition is applied to the gradients calculation. Synthetic example on the Sigbee2A model proves the validity of our method for recovering the long wavelength components of the model.

Introduction

Elastic full waveform inversion provides high-resolution model estimation but notoriously surfers from the nonlinearities of multi-parameter inversion and also the same cycle-skipping problem as in acoustic case (Sears et al., 2008; Brossier et al., 2009). Xu et al. (2012) suggested using a reflection waveform inversion (RWI) method, which aim to invert the long-wavelength components of the model by using the reflections predicted by migration/demigration process. Through minimizing misfit function of waveform, the RWI method are developed by several work (Wu and Alkhalifah, 2015; Zhou et al., 2015), and recently extended to elastic case by Guo and Alkhalifah (2016).

However, traveltime information are more sensitive and linearly related to low-wavenumber model perturbation. Using traveltime inversion will be more robust and helpful to build appropriate initial models containing long-wavelength components for conventional FWI (Ma and Hale, 2013; Chi et al., 2015; Luo et al., 2016). Unfortunately, in elastic case, traveltimes of a particular wave modes are difficult to extract due to the complicated mode-conversions. In this abstract, we aim to tackle the traveltime misfits of P-P and P-S reflections with the help of wave mode decomposition and dynamic image warping (DIW) (Hale, 2013). Then, we use the traveltime of P-P and P-S reflections to implement the WERTI method (Ma and Hale, 2013) with a two-stage workflow. Finally, the numerical example of Sigsee2A model proves the robustness and validity of our elastic WERTI method.

Objective function and gradients of elastic WERTI

Assume that there is a perturbation δc_{ijkl} in the background elastic media c_{ijkl}, the background wavefileds u_i and perturbed wavefields δu_i satisfy:

$$\rho\frac{\partial u_i^2}{\partial t^2}-\frac{\partial}{\partial x_j}\left[c_{ijkl}\frac{\partial u_k}{\partial x_l}\right]=f_i, \tag{1}$$

and

$$\rho\frac{\partial \delta u_i^2}{\partial t^2}-\frac{\partial}{\partial x_j}\left[c_{ijkl}\frac{\partial \delta u_k}{\partial x_l}\right]=\frac{\partial}{\partial x_j}\left[\delta c_{ijkl}\frac{\partial u_k}{\partial x_l}\right], \tag{2}$$

where δu_i can be seen as the demigrated reflection data using the image perturbation δc_{ijkl} obtained from RTM or other image method. In WERTI, we aim to minimize the traveltime differences between observed data $\mathbf{d}^o$ and calculated data $\mathbf{d}^c$, then the objective function is:

$$E=\frac{1}{2}\int \tau^2(\mathbf{x_r},t;\mathbf{x_s})dtd\mathbf{x_r}d\mathbf{x_s}, \tag{3}$$

where the time differences $\tau(\mathbf{x_r},t;\mathbf{x_s})$ can be extracted through DIW. After a similar derivation as in Ma and Hale (2013), the gradients of equation (3) can be expressed as:

$$\frac{\partial E}{\partial c_{ijkl}}=-\int(\frac{\partial u_i}{\partial x_j}\frac{\partial \delta\psi_k}{\partial x_l}+\frac{\partial \delta u_i}{\partial x_j}\frac{\partial \psi_k}{\partial x_l}), \tag{4}$$

where ψ_i and $\delta\psi_i$ are the adjoint wavefields satisfying:

$$\rho\frac{\partial \psi_i^2}{\partial t^2}-\frac{\partial}{\partial x_j}\left[c_{ijkl}\frac{\partial \psi_k}{\partial x_l}\right]=\tau(\mathbf{x_r},t;\mathbf{x_s})\frac{\dot{d}_i^o(\mathbf{x_r},t+\tau;\mathbf{x_s})}{h_i(\mathbf{x_r},t;\mathbf{x_s})}, \tag{5}$$

and

$$\rho\frac{\partial \delta\psi_i^2}{\partial t^2}-\frac{\partial}{\partial x_j}\left[c_{ijkl}\frac{\partial \delta\psi_k}{\partial x_l}\right]=\frac{\partial}{\partial x_j}\left[\delta c_{ijkl}\frac{\partial \psi_k}{\partial x_l}\right], \tag{6}$$

with $h_i(\mathbf{x_r},t;\mathbf{x_s})=(\dot{d}_i^o(\mathbf{x_r},t+\tau;\mathbf{x_s}))^2-\ddot{d}_i^o(\mathbf{x_r},t+\tau;\mathbf{x_s})(d_i^c(\mathbf{x_r},t;\mathbf{x_s})-d_i^o(\mathbf{x_r},t+\tau;\mathbf{x_s}))$. The hat dot denotes the time derivative. On the right hand side (RHS) of equation (4), the first and second term indicate the source and receiver part of the reflection wave-path, respectively. Then we can get the gradients in terms of P- and S- wave velocities through the chain rule:

$$\frac{\partial E}{\partial V_p}=2\rho V_p\frac{\partial E}{\partial c_{ijkl}}\delta_{ij}\delta_{kl},\qquad \frac{\partial E}{\partial V_s}=2\rho V_s\frac{\partial E}{\partial c_{ijkl}}(-2\delta_{ij}\delta_{kl}+\delta_{ik}\delta_{jl}+\delta_{il}\delta_{jk}). \tag{7}$$

Workflow of elastic WERTI

In elastic case, it is common to observe that different mode-conversions, mainly P-P and P-S events, overlap and intersect with each other. The cross points between events would be singularities for traveltime difference estimation through DIW. Therefore, $\tau(\mathbf{x_r}, t; \mathbf{x_s})$ would be inaccurate if using the original multicomponent seismic data, which makes the above gradients difficult to implement. To deal with this, we decompose the observed and calculated data into P- and S-wave parts, respectively. The decomposition is only applied on the surface recording data (Li et al., 2016) so that we can easily get the separated vector P and S-wave seismograms for each shot. In this way, the traveltime differences can be divided into P- and S-wave part, with which we can implement the elastic WERTI through a two-stage workflow, i.e. the P-wave stage followed by the S-wave stage.

In the P-wave stage, the P-P reflections are mainly used to build the P-wave velocity model. Firstly, we obtain the perturbation of V_p (δV_p) through elastic reverse time migration (ERTM). Since only the traveltime is considered in WERTI, we just apply an ERTM to obtain the image rather than a least-square ERTM to fit the amplitude of reflections. Then, the objective function is changed to minimize the P-P reflection traveltime differences:

$$E_{pp} = \frac{1}{2} \int \tau_{pp}^2(\mathbf{x_r}, t; \mathbf{x_s}) dt d\mathbf{x_r} d\mathbf{x_s}. \tag{8}$$

Thus, we can obtain the gradient of V_p, $\frac{\partial E}{\partial V_p}$, just using the P-wave seismograms to calculate RHS of equation (5) and replacing δc_{ijkl} with δV_p in equation (2) and (6).

In the S-wave stage, a similar strategy is applied using the P-S reflection traveltime. The objective function becomes:

$$E_{ps} = \frac{1}{2} \int \tau_{ps}^2(\mathbf{x_r}, t; \mathbf{x_s}) dt d\mathbf{x_r} d\mathbf{x_s}. \tag{9}$$

However, the implementation is a little different from the previous stage. After the P-wave stage inversion, the background V_p should be well recovered. As we know, in most cases V_p and V_s share a same structure in the subsurface. Therefore, we recommend to use the well imaged δV_p instead of δV_s to generate the P-S reflections. Besides, in the P-S reflection, the source part of the wavepath only relates to P-wave velocity so that we can drop the first term in the RHS of equation (4) when calculating $\frac{\partial E}{\partial V_s}$. And also wave mode decomposition is applied to make sure that only S-wave energy are involved:

$$\frac{\partial E_{ps}}{\partial V_s} = -2\rho V_s \int (\frac{\partial \delta u_i^S}{\partial x_j} \frac{\partial \psi_k^S}{\partial x_l})(\delta_{ik}\delta_{jl} + \delta_{il}\delta_{jk}). \tag{10}$$

The above gradient is similar to the EFWI proposed by Wang et al. (2015). The mode decomposition can mitigate parameter trade-offs and suppress artifacts for the V_s inversion.

Sigbee2A model example

The synthetic example involves a part of the Sigsbee2A model (Figure 1a and 1b). The V_s model is generated using fixed Poisson's ratio. Figure 1c and 1d show the initial model of V_p and V_s, which linearly increase with depth. We can see the initial model of V_p is lower while the initial model of V_s is higher than the true model, but both of them is far from the true value. 36 shots are evenly deployed on the surface with a maximum offset of 4km. Pure P-wave source is used with a main frequency of 15Hz.

Figure 2a and 2b show the inverted results of elastic WERTI. Since the linearly increased initial model is quite far from the true value, certainly there will be cycle-skipping problem if we use this for conventional EFWI. However, after 40 iteration for each stage, WERTI provides a good recovery of the background information for both V_p and V_s. Using the inverted results of WERTI as starting models, we also perform the conventional EFWI. As shown in Figure 2c and 2d, both of the inverted V_p and V_s models are well reconstructed except the right part. The reason should be that, on the right part, the reflection coverage of surface observation is insufficient for WERTI to rebuild the long-wavelength components. Figure 3 shows the vertical profiles at 1.5km and 3km. We can see that the elastic WERTI provides reliable starting models containing long-wavelength components for EFWI and the EFWI results match well with the true value.

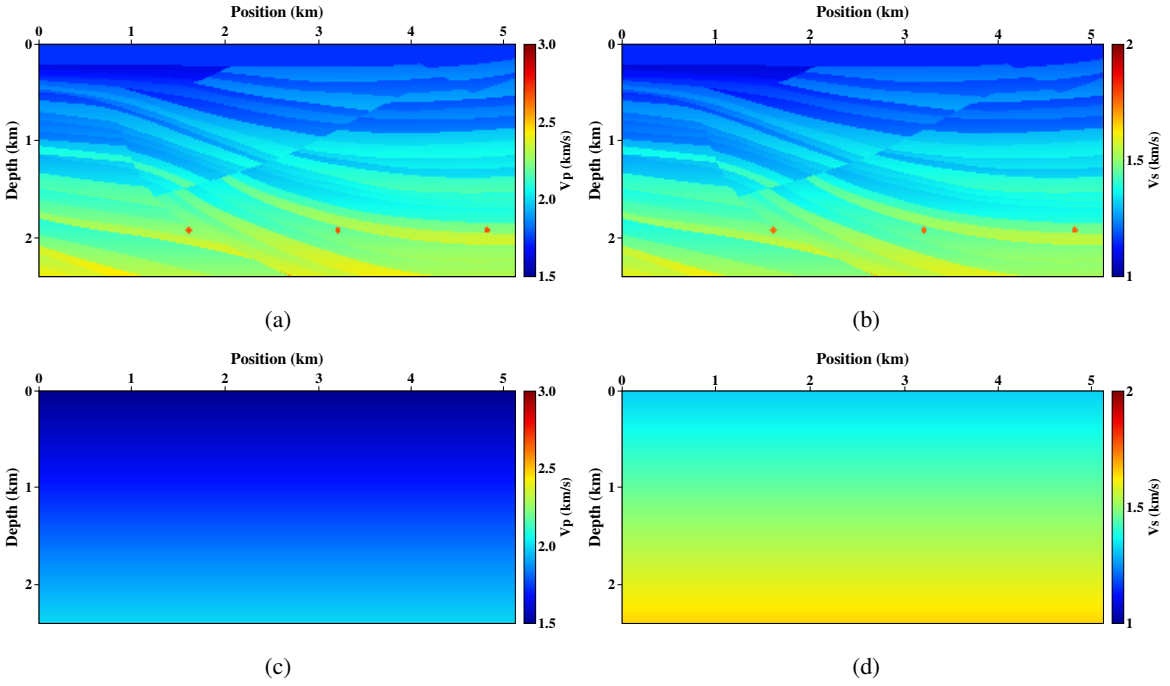

Figure 1: Sigbee2A model example. On the top are true models of V_p (a) and V_s (b). On the bottom are initial models of V_p (c) and V_s (d) linearly increasing with depth.

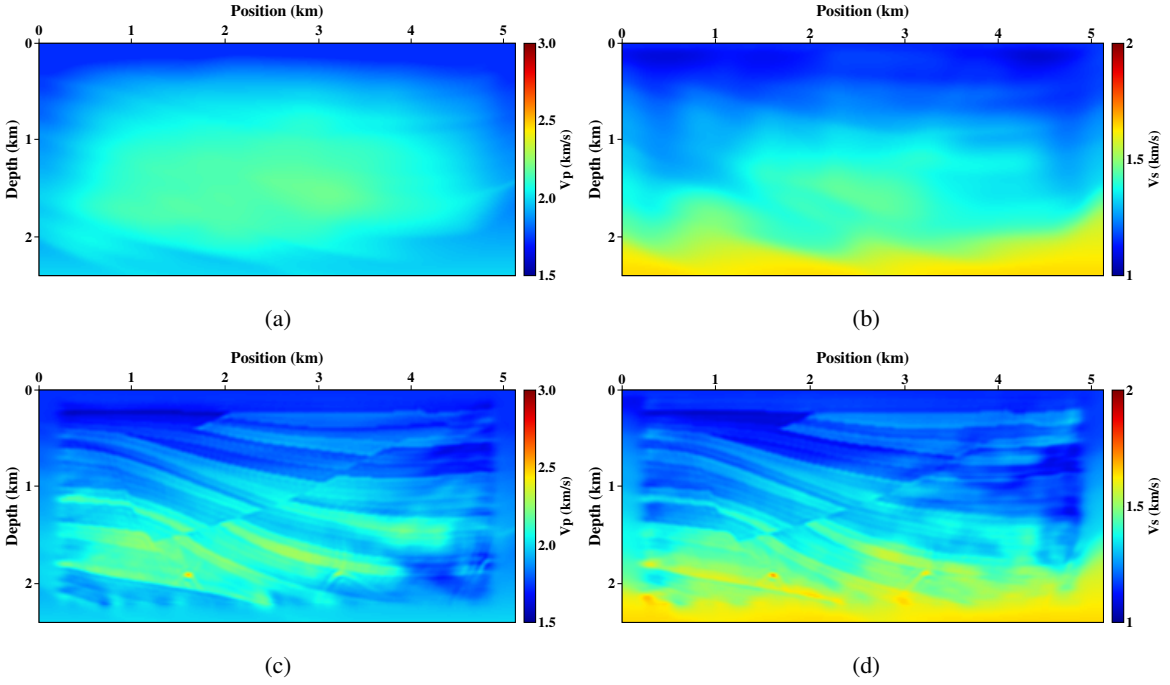

Figure 2: Inverted results of WERTI and EFWI. (a) and (b) are inverted V_p and V_s model through two-stage elastic WERTI with the linearly increased models as initial models. (c) and (d) are inverted V_p and V_s through EFWI using (a) and (b) as starting models.

Conclusions

Reflection traveltime inversion only minimizes traveltime misfits which are more sensitive and linearly related to the low-wavenumber model perturbation. With the aid of DIW and P/S separation of 3C seismograms, we can obtain the travel time differences of P-P and P-S reflections, respectively. To build

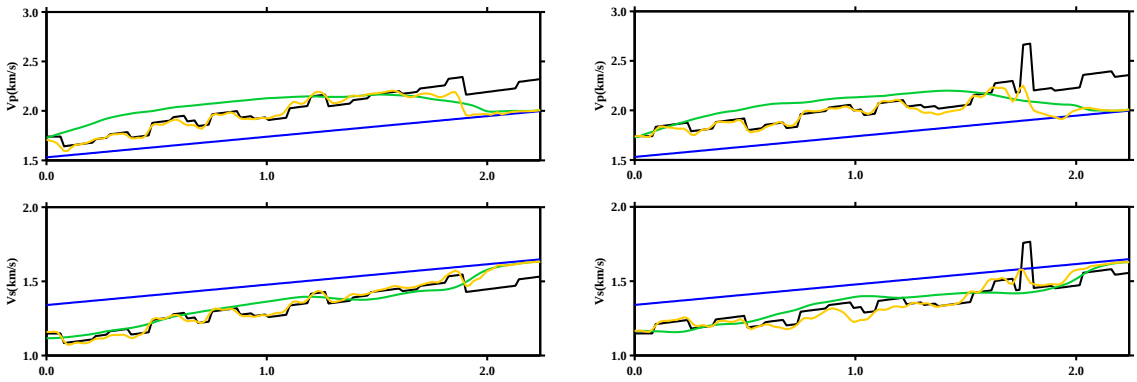

(a) (b)

Figure 3: Vertical profiles of elastic WERTI and EFWI results at 1.4km (a) and 3km (b). The black and blue lines indicate the true and linearly increased initial model. The green and yellow lines indicate the WERTI and EFWI results, respectively.

the long-wavelength component of the model, we introduce a two-stage WERTI workflow by firstly using P-P then P-S reflections. In the second stage, the wave mode decomposition can mitigate parameter trade-offs and suppress artifacts when calculating gradient of V_s. The Sigsbee2A model example proves that even starting with a bad initial model, the two-stage elastic WERTI strategy can provide reliable starting model for conventional EFWI.

Acknowledgement

This work is supported by the National Natural Science Foundation of China (NO.41474099, 41674117 & 41630964). This paper is also based upon the work supported by the King Abdullah University of Science and Technology (KAUST) Office of Sponsored Research (OSR) under award NO. 2230. We appreciate the open-source package of DENISE from *https://github.com/daniel-koehn/* and Mines Java Toolkit from *https://github.com/dhale*. We thank the useful advice from Tariq Alkhalifah (KAUST), Zedong Wu (KAUST) and Benxin Chi (Los Alamos).

REFERENCES

Brossier, R., S. Operto, and J. Virieux, 2009, Seismic imaging of complex onshore structures by 2d elastic frequency-domain full-waveform inversion: Geophysics, **74**, WCC105–WCC118.

Chi, B., L. Dong, and Y. Liu, 2015, Correlation-based reflection full-waveform inversion: GEOPHYSICS, **80**, R189–R202.

Guo, Q., and T. Alkhalifah, 2016, *in* A nonlinear approach of elastic reflection waveform inversion: Society of Exploration Geophysicists, 1421–1425.

Hale, D., 2013, Dynamic warping of seismic images: GEOPHYSICS, **78**, S105–S115.

Li, Z., X. Ma, C. Fu, B. Gu, and G. Liang, 2016, Frequency-wavenumber implementation for p- and s-wave separation from multi-component seismic data: Exploration Geophysics, **47**, 32.

Luo, Y., Y. Ma, Y. Wu, H. Liu, and L. Cao, 2016, Full-traveltime inversion: GEOPHYSICS, **81**, R261–R274.

Ma, Y., and D. Hale, 2013, Wave-equation reflection traveltime inversion with dynamic warping and full-waveform inversion: GEOPHYSICS, **78**, R223–R233.

Sears, T., S. Singh, and P. Barton, 2008, Elastic full waveform inversion of multi-component OBC seismic data: Geophysical Prospecting, **56**, 843–862.

Wang, T., J. Cheng, and C. Wang, 2015, Elastic wave mode decoupling for full waveform inversion: Presented at the 77th EAGE Conference and Exhibition 2015, EAGE Publications.

Wu, Z., and T. Alkhalifah, 2015, Simultaneous inversion of the background velocity and the perturbation in full-waveform inversion: GEOPHYSICS, **80**, R317–R329.

Xu, S., D. Wang, F. Chen, G. Lambare, and Y. Zhang, 2012, Inversion on reflected seismic wave: 82nd Annual International Meeting, SEG, Expanded Abstracts, 1–7.

Zhou, W., R. Brossier, S. Operto, and J. Virieux, 2015, Full waveform inversion of diving & reflected waves for velocity model building with impedance inversion based on scale separation: Geophysical Journal International, **202**, 1535–1554.